Hydrophobic and Antibacterial Activity of Silk Textile Surfaces Using Reduced Graphene Oxide (RGO) and TiO_2 Coating

Mahamasuhaimi Masae [a,*], Lattapon Sengyi [a], Likhit Wanapong [b], Parnumart Choopool [c], Pirapon Potipongsa [d]

[a] *Department of Industrial Engineering, Faculty of Engineering, Rajamangala University of Technology Srivijaya, Songkhla, 90000 Thailand*
[b] *Department of Industrial Technology, Faculty of Engineering, Rajamangala University of Technology Srivijaya, Songkhla, 90000 Thailand*
[c] *Department of Mining and Materials Engineering, Faculty of Engineering, Prince of Songkla University, Songkhla, 90112 Thailand*
[d] *Department of Technologies and Equipment for Materials Processing, Faculty of Materials Science & Engineering, "Gheorghe Asachi" Technical University of Iasi, 700050 Romania*

Received 12 June 2018; Revised 27 August 2018; Accepted 31 August 2018

Abstract

This study aims to investigate the structure and functional properties of reduced graphene oxide (RGO) doped with TiO_2 nanomaterials based on the modified cellulose fibers of silk. The RGO and TiO_2 nano-particulates were prepared by modified Hummer's and sol-gel methods, respectively. The study also investigated the efficiency of this coated silk fabrics to inhibit the growth of bacteria: *Escherichia coli* (*E. coli*) and *Staphylococcus aureus* (*S. aureus*). The coated silk fabrics were analyzed using X-ray diffraction (XRD), Scanning electron microscopy (SEM), Fourier transform infrared spectroscopy (FTIR) and contact angle meter. The highest observed water contact angle was at 139 degree with the highest loading of graphene oxide. The fabric surfaces grafted with RGO also exhibit adhesive type hydrophobicity. The antibacterial activities against *E. coli* and *S. aureus* were about 98 and 93% respectively under ambient temperature that showed RGO doped TiO_2 nano-particulates film enhance bacterial inactivation within textile standard. The expected overall properties of nanocomposites may open the way towards new applications of high performance fabrics, leading to an innovative product development in the textile industry, hospitals, electronics for coatings and many other applications.

KEYWORDS: Sol-gel; Antibacterial activity; Low temperature TiO_2 preparation

* Corresponding authors; e-mail: asusumeme1983@yahoo.com

Introduction

Self-cleaning surface receives great attention around the world due to its wide range of practical applications. For example, self-cleaning technology has been successfully used in the field of textiles and a great variety of self-cleaning textile products have also been commercialized. Generally, self-cleaning textiles can be realized by two strategies: superhydrophobicity induced self-cleaning and photocatalysis induced self-cleaning. Superhydrophobic textiles show a large water contact angle and therefore repel water. Moreover, contaminates adhered to the surface can be removed easily by the passage of flowing liquids. Long chain perfluorinated chemicals have been widely used to achieve superhydrophobicity because of their ultra-low surface energy [1]. The second class of self-cleaning textile is photocatalytic coating which can chemically break down organic dirt to carbon dioxide, water and mineral acids when exposed to light, a process known as photocatalysis [2 – 7].

A single layer Graphene and the few layer Reduce graphene oxide (RGO) of sp^2-bonded carbon atoms tightly packed into a two-dimensional honeycomb structure, has attracted a lot of attention since its discovery in 2004, due to its outstanding mechanical, thermal, optical, and electrical properties. [8] In the recent years, TiO^2 was also investigated for photocatalytic degradation of organic contaminants. Titanium dioxide (TiO_2) has three crystal forms namely, Anatase, Rutile and Brookite. Efficient photocatalytic activity of TiO_2 deeply depends on its crystallite size, surface area,

and crystal structure [9]. As widely reported, Anatase and mixture phases of Anatase and Rutile display highest photocatalytic activities [10 – 11]. Anatase, with large surface area, high crystallinity and nano-scaled crystallite size, exhibits high photocatalytic activity. In the process, oxygen atoms are ejected, and oxygen vacancies are created in the ground state. These holes can oxidize the O anions. Water molecules can then occupy these oxygen vacancies to produce adsorbed OH groups. For the past twenty years, the novel microbiocidal activities of TiO_2 through a photocatalytic reaction over E. coli [12], S. aureus [13], virus and cancer cells [14] have been reported. Furthermore, the application of TiO_2 photocatalytic disinfection for drinking water production has been investigated, and the development of incorporating TiO_2-coated for food packaging and food preparation equipment has also received attention. Nowadays, coated textiles are being widely used in clothing and garment industry. Thus, RGO-TiO_2 (GT) nanocomposites have become a promising material for photocatalytic applications. GT has high stability, high photocatalytic activity, and enhanced photovoltaic properties [15] because of its enhanced quantum efficiency and decreased band gap energy [16]. Several studies have been focused on the photocatalytic activity of RGO and graphene. The modification of TiO_2 by doping with graphene with high photocatalytic activity more than pure TiO_2 for the degradation of sodium pentachlorophenol [17]. In 2015, Qinqin et al. [18] demonstrated that the highly hydrophobic solid contact based on graphene-hybrid nanocomposites for all solid state potentiometric sensors with well-formulated phase boundary potentials [18]. In addition, cotton fabrics coated with TiO_2-SiO_2 composite particles exhibit superhydrophobicity with a water contact angle of 160.5°. However, the superhydrophobic cotton fabrics can be easily wetted by oil dirt and become superhydrophilic. Herein, the TiO_2-SiO_2 composite particle coated cotton fabric, which was contaminated with oleic acid, can recover its superhydrophobicity after UV irradiation for 4 h. [19]. In particular, hydrophobic properties on cotton fabric was successfully achieved for the first time by grafting graphene oxide on the fabric surface, using a dyeing method [20].

In the present study, RGO of different loading ratios were prepared. Then non-aqueous synthesis of high purity TiO_2 nanocrystals was carried out in the presence of ormosil particles and GT composite particles were finally obtained by coating GT nanocrystals onto silk fabrics at room temperature. Hydrophobicity was measured using water contact angle on silk fabric as a function of RGO loading. The surface of silk was also characterized using spectroscopic and microscopic methods. Based on these results a mechanism is proposed to explain the hydrophobic properties observed. The antimicrobial capacity of this coated silk against *E. coli* and *S. aureus* exposed in vitro tests has been determined.

Materials and Methods

Preparation of aqueous graphene oxide (RGO) dispersion

Firstly, GO was prepared by using the modified Hummer's method [21], 1 g of natural Graphite flake (–10 mesh, 99.9%, Alfa Aesar), 0.5 g of $NaNO_3$ (Ajax Finechem) and 23 ml of sulfuric acid (98%, J.T. Baker) were mixed and stirred in ice bath for 30 min. 3 g of potassium permanganate ($KMnO_4$, Ajax Finechem) was slowly added to the stirred suspension and kept the temperature below 20 °C for 30 min. Then the solution was stirred at 35 °C for 24 h, turn to brownish-gray past. After that, 40 ml of distilled water was added to the mixture then the temperature reached >90 °C, stirred for 30 min. After cooled, added 10 ml of H_2O_2 and 140 ml of distilled water, stirred for 15 min. The product was filtered, washed with water, 1M HCl and ethanol. Finally, graphene oxide powder was collected and dried at 80 °C for 24 h. Second, GO reduction by the chemical reduction method [22 – 24]. 0.5 g of GO, 100 ml of 0.5% NH_4OH (37%, J.T. Baker) were mixed and stirred at 60 °C for 30 min, the dispersion turned yellow-brown that 4 mM of ascorbic acid (99.5%, Poch) was mixed and kept the temperature at 95 °C for 60min. The mixture were filtered and washed by distilled water and ethanol until pH ~6 then the powder was collected and mixed with 100 ml of distilled water for making a dispersion of 5 mg ml^{-1} RGO

Preparation of TiO_2 sol and GT nano platelets

Titanium (IV) isoproxide (TTIP, 99.95%, Fluka Sigma-Aldrich) was used as starting materials. The TiO_2 sol was synthesized by adding the mixture of TTIP (9.0 ml) with 143.0 ml ethanol (99.9%; Merck Germany), stirring at room temperature with a speed of 800 rpm for 30 min to achieve the mole ratio of TTIP:C_2H_5OH = 1:82 then adding 10 ml glacial acetic acid into the sol to adjust pH to be about 3.0. GT nano platelets prepared at different RGO dispersion ratios while TiO_2 sol dosages were fixed at 10 ml (Table 1).

Preparation of silk fabric dyed with GT nano platelets

The silk fabrics samples scoured and bleached (81.4 gm^{-2}, plain weave) were dipped in different concentrations of GT dispersions for 45 min. This allows the GT sheets to be deposited on silk fabric surface in the form of thin films. Different methods have been reported to deposit thin films containing graphene oxide sheets on substrates [20]. The silk fabrics were then removed and send through two rotating rollers (padding rollers) which apply a uniform pressure along the surface of the fabric to remove excess water. Padding roller pressure on fabric was kept at a constant value where fabric's weight gain after padding was kept at 100wt% gain. GT loaded silk samples were labeled as shown in Table 1 according to the concentration of GT in the aqueous solution as shown in Table 1. The treated samples were then dried using an oven at 60 °C for 1 h.

Table 1 Summary of the experimental conditions and different GT concentration in water for loading on the silk fabrics.

Sample	RGO concentration (mg ml^{-1})	TiO_2 Sol (ml)
1.0G	1.0	–
10T	–	10
0.4GT	0.4	10
0.6GT	0.6	10
0.8GT	0.8	10
1.0GT	1.0	10

Materials Characterization

The X-ray thin film diffraction (XRD) patterns were characterized in terms of phase compositions and crystallite size by using an x-ray diffractometer, Phillips X'pert MPD, CuKα. The crystallite size was determined from XRD peaks using the Scherer's equation (1) [25],

$$D = 0.9\lambda / \beta \cos\theta_\beta \quad (1)$$

Where D is crystallite size, λ is the wavelength of the x-ray radiation (CuKα = 0.15406 nm), and β is the angle width at half maximum height, and θ_β is the half diffraction angle of the centroid of the peak in degree. Hydrophobic properties of the films in terms of contact angles and hydrophobicity were investigated under visible light using a contact angle meter (OCA15EC). The FTIR transmittance spectra of the samples were also analyzed in order to confirm hydroxyl function group (TiO_2-OH bonds) of the films. The band gap energy value of sample in the powder form was measured by UV Vis-NIR Spectrometer with integrating sphere attachment (ShimadzuISR-3100 spectrophotometer by using $BaSO_4$ as reference). The surface morphology of the prepared films was characterized by scanning electron microscopy (SEM, FEI Quanta 400).

Antibacterial activity of silk fabric coated with nanocomposite

Antibacterial activity was characterized in terms of percentage reduction in visible growth of bacteria. For a qualitative, relative and easily executed method to determine residual antibacterial activity of textile materials, refer to AATCC Test Method 100-2004. Typical gram positive and gram negative micro-organisms *S. aureus* (ATCC 6538) and E. coli O157:H7 (ATCC 43895) (American Type Culture Collection, Rockville, MD). The Trypticase soy agar was from DifcoLaboratories, Detroit, MI. The initial bacterial concentration was kept about 105 CFU ml^{-1} used for all experiments. The percentage reduction in the number of colony forming units between the untreated and treated fabrics after incubation for 24 h at 37 ± 1 °C was calculated using the following equation (2)

$$R = 100(B - A) / B \quad (2)$$

Where R is the percentage reduction in bacteria, and B and A are the numbers of CFU ml^{-1} of bacteria measured for the untreated and the treated silk fabrics respectively.

Results and Discussion

Nanocomposite structure

XRD was carried out to identify the crystal structure of pure TiO_2 and RGO samples. From the XRD study as shown in Fig. 1, the Anatase peaks were observed at 25.50°, 37.59°, 48.01°, 53.88° and 62.48°, and the patterns show peaks attributed to (101), (004), (200), (105) and (204), respectively. The XRD pattern of RGO is shown in Fig. 1. It is found that the characteristic diffraction peak of GO at ~ 10° disappears in RGO, which demonstrates that the GO was reduced to RGO during the heat treatment. The RGO XRD pattern consists basically of two peaks located at around 26° and 43°, corresponding to the (002) diffraction of the graphitic layered structure and the (100) diffraction for graphite, respectively. The XRD pattern of RGO is typical of nongraphitic carbon materials with a highly disordered nanocrystalline structure. In addition, the samples show a low signal to

background ratio, which is probably attributable to incoherent scattering from noncrystalline materials. It is unavoidable that large amounts of hydrocarbons, impurities, and heteroatoms are formed on the graphene surfaces during the oxidative process in strong acid in the modified Hummers' method [26]. This consequently results in the smaller grain size of TiO_2 (15.8 nm) film compared to those of RGO (19.4 nm).

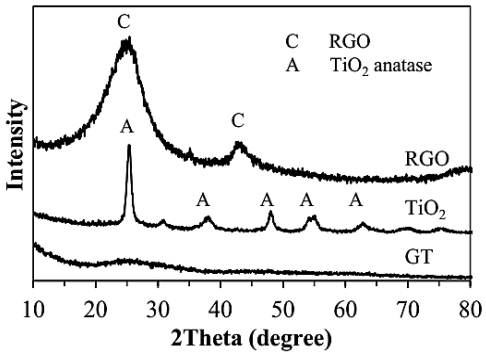

Fig. 1 XRD patterns of TiO_2, RGO and GT coated on silk fabric.

Hydrophobic property

Contact angle measurements of film surface carried out in ambient air environments. The contact angle of water droplets on the film surface of graphite oxide coated silk fabric at different RGO loadings in Fig.2. Maximum loading of RGO which consist of many layers of RGO on silk fabric results in hydrophobicity with an average water angle of 139°.

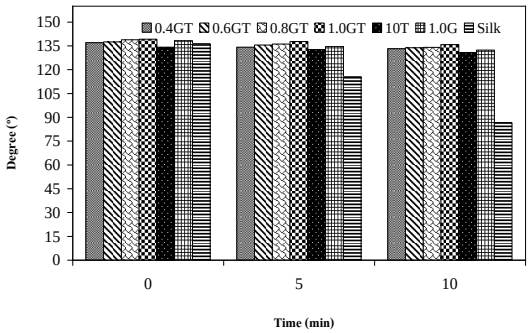

Fig. 2 Water contact angles vs. time of GT composite coated on silk fabrics.

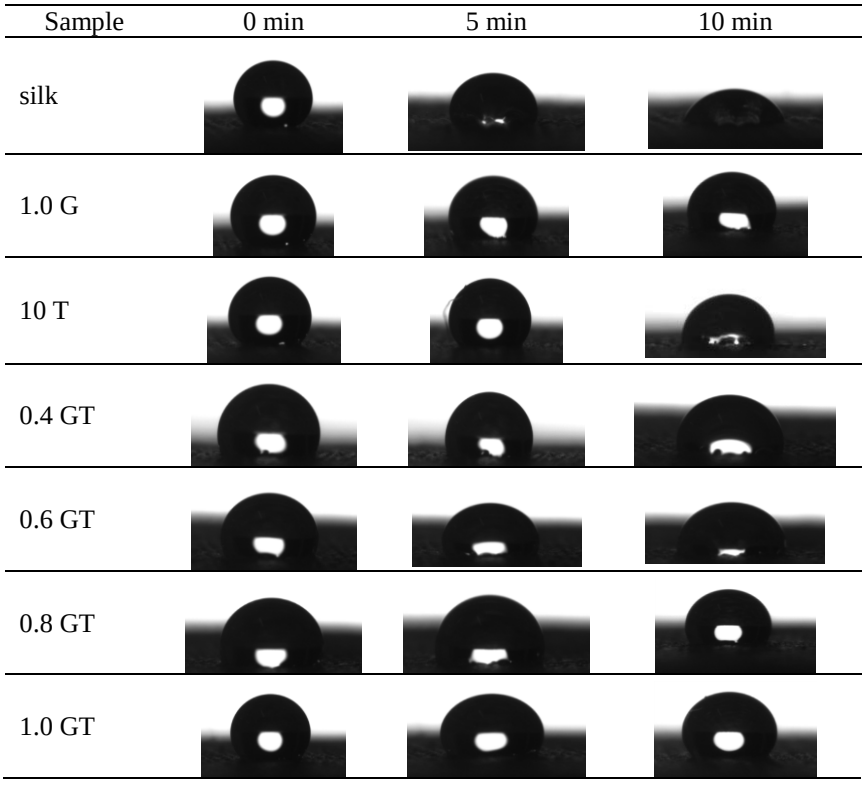

Fig. 3 Images of water droplets on composite coated silk fabric at 0, 5 and 10 min.

It was found that RGO loading has a significant effect on increasing the contact angle of water droplets due to their enhancement that RGO sheets loaded on silk fabrics are able to make loading amount and degree of hydrophobicity on the textile surface compared to that of the pure TiO_2 film. Fig. 3 shows the change in water contact angle as the RGO loading on the fabric surface increases. As shown in Fig. 3 when we expose the GT composite coated silk textile (sample 0.4 GT, 0.6 GT, 0.8 GT and 1.0 GT) the water droplets remain displayed larger contact angles on the surface. Hydrophobicity (contact angle = 135°) of the GT composite film was observed at 10 min (Figs. 2 and 3). The coating has successfully produced an adhesive type hydrophobicity which is similar to hydrophobicity present in the lotus effect.

Surface Morphology of Silk Coated composite materials

The surface morphologies of GT are shown in Fig. 4 a – d together with EDX analysis of a representative sample Table 2. The morphology of pure silk fibers does not contain any contaminations (Fig. 4a). The silk fibers in the 1.0 G are unevenly covered by RGO nanoflakes after coated by GT (Fig. 4b). The sample 10T obtained with the use of the sol also contains TiO_2 particles (Fig. 4c). Fig. 4d shows that the RGO doped TiO_2 nanoparticle aggregates with flake RGO are unevenly covered. The quantitative EDX analysis form the coated silk fibers and the presence of RGO and TiO_2 are shown in Table 2. The elements Ti, O and C were clearly detected and the quantitative analysis estimated weight fractions in this order were about 20.19, 31.86 and 55.36wt%, for the GT surface. In addition, the composite samples show a low carbon ratio, which is probably attributable to hydrocarbons are lost on the graphene surfaces during the oxidative process in strong acid in the TiO_2 sol gel process.

Table 2 The EDX results of TiO_2, RGO and GT coated silk fabric.

Element (wt%)	Silk	Silk coated RGO	Silk coated TiO_2	Silk coated GT
C	68.20	69.99	47.95	55.36
O	31.98	30.01	31.80	31.86
Ti	–	–	12.84	20.19

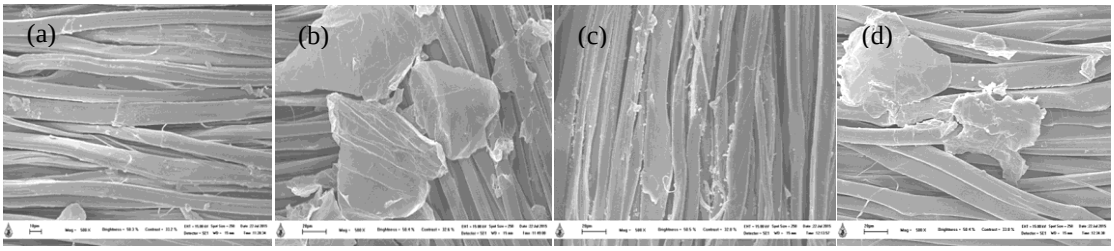

Fig. 4 SEM micrographs: silk (a), 1.0G (b), 10T (c), and 1.0GT (d).

FTIR analysis

Fig.5 shows the FTIR spectra of representative RGO, TiO_2 and GT samples. The FTIR spectra reveal that GT and reference TiO_2 sample that exhibits absorbance bands in the range 3100 – 3700 cm^{-1} indicative of the stretching vibration of -OH or absorbed water molecules [27]. The band at 1630 cm^{-1} was attributed to the bending vibrations of the O-H bond, it has been reported that more hydroxyl groups existing on the titania surface favors the enhancement of the photocatalytic activity. The stronger absorbance peak around 800 – 550 cm^{-1} is corresponding to the vibration of Ti-O and the Ti-O-Ti bridging stretching modes [27]. Each spectrum of RGO presents typical modes related to oxygen containing functional groups. The band at ~1100 cm^{-1} corresponds to C-O stretching vibration of the alkoxy groups. The mode at 1160 cm^{-1} arises from C-O-C stretching vibration of the epoxy groups. The mode at 1467 cm^{-1} is attributed to C-OH stretching vibration of the carboxyl group. The peak at 1710 cm^{-1} arises from the C=O stretch of the carboxyl group and at 3440 cm^{-1} from O-H groups [28 – 29]. Furthermore the band appeared at 1100 cm^{-1} and bands below 1000 cm^{-1} correspond to Ti-O and Ti-O-Ti stretching, respectively. In addition, new bands appeared at approximately 650, 710 and 900 cm^{-1}, which can be assigned to Ti-O-Ti and Ti-O-C vibrations [30 – 31]. These results confirm the presence of hydroxyl group generated by photocatalytic reaction of the catalyst in the structure of films. The hydroxyl group and

absorbed water are fruitful to photocatalytic reaction since they react with photo generated holes on TiO_2 surfaces to produce hydroxyl radicals, which are powerful oxidant [32]. This suggest that when RGO loading on the fabric sample increases it contains more hydrophobic area (C=C) compared to hydrophilic areas (C-O-C, R-O-O-R). The contact angle measurement, the silk fabric samples loaded with higher amount of RGO shows the best hydrophobicity of 139°. RGO sheets have their own hydrophilic and hydrophobic functionalities which are directly related with the layer size and the degree of oxidation of the graphite. A single layer of RGO has both hydrophobic and hydrophilic sites making it a two dimensional amphiphilic structure. As an amphiphilic material, RGO has an edge-to-center distribution of hydrophilic and hydrophobic domains. We propose that the edge sites are more hydrophilic while the mid sheet regions which are dominantly made up of C=C bonds are hydrophobic [20].

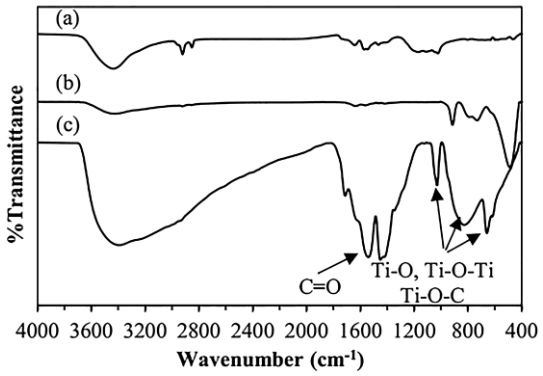

Fig. 5 FTIR spectra of RGO (a), TiO_2 (b) and 1.0GT composite (c)

Energy gap measurement

The UV-vis spectra of pureTiO_2, RGO and composite materials shown in Fig. 6. The band gap energies (E_g) of the samples was determined and analyzed by intercept x of the linear portion of $(\alpha hv)^2$ as a function of E to $\alpha E=0$ (where $E=E_g$) of following equation (3) [19]

$$\alpha E = A'(E - E_g)^m \quad (3)$$

where E_g is the band gap energy (eV) of the sample and λ is the wavelength of the on set of the spectrum (nm). ($E = hc/\lambda$), respectively. M = 1/2 for direct band gap and m = 2 for indirect band gap. The absorption coefficient (α) was calculated by $\alpha = A/d'$ where A is the measured absorbance (nm), d' is the thickness of samples in UV-vis cell (0.4 cm) [19]. It can be seen that most dopants have an effect on the UV-vis spectra due to an inhibition of the recombination of electron-hole pairs [33], especially in the case of GT samples. The sharp decrease in the optical transition and long tail is probably caused by lattice defects such as oxygen vacancies [17, 34]. The RGO show a spectrum shape with strong adsorption at visible light region due to their similar black appearance. At a wavelength below 400 nm, the GT and RGO have a much weaker absorption and different shape in comparison with pure TiO_2 samples. As shown in Fig. 6, But at the visible light, the absorption intensity of GT is stronger than pure TiO_2 due to the presence of 1.0 mg ml^{-1} RGO in the GT composite.

From Fig. 6 (right), the band gap energies of GT compared with pure TiO_2 decreased from 3.40 to 3.20 eV and RGO displayed the highest band gap energy about 1.75 eV. This change demonstrates

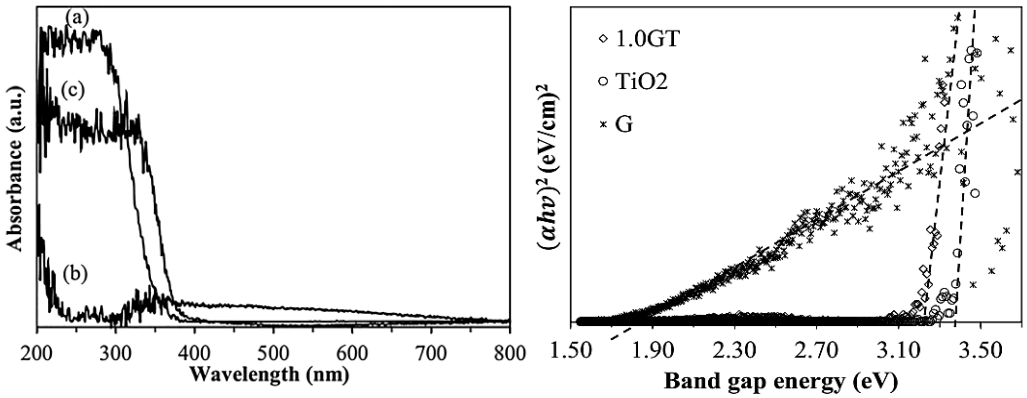

Fig. 6 UV-vis diffuse reflectance spectra (left) and Band gap energies (right) of (a) pure TiO_2 (b) RGO and (c) 1.0GT powders

a strategy for mediating photocatalysis through an atomic level doping for nanocatalyst. In addition, the absorption capacity spectra of the GT samples also showed a larger amount of visible light absorption than pure TiO_2 [17, 34], indicating that RGO doping may be a promising approach to an increase in the catalytic activity under visible light. It can be seen that the absorption wavelength of the composite sample is extended greatly towards visible light, compared with TiO_2 and RGO samples [17], as well as pure TiO_2, resulting in the highest photocatalytic activity. This effect of RGO doping in TiO_2 on enhancement of visible light absorption capacity agrees well with the previous works [17, 34].

Antibacterial activity of silk surface coated with nanocomposite

The aim of this study was to evaluate the antibacterial activity of GT. The silk fabrics dyed with composite materials were tested for against *E. coli* and *S. aureus*. The results were compared between the controls and the best hydrophobic properties materials, 1.0 GT under UV light activation. Each test was performed in triplicates. Textiles have long been recognized as a media to support the growth of bacteria as they provide excellent environment for bacterial growth. The antibacterial textiles can protect not only the textile itself from damage but also the textile user against pathogenic or odor causing bacteria. So it is highly desirable that the growth of bacteria on textiles is minimized in their use and storage [35, 36]. It is fortunate to discover the antibacterial activity of GT. The viable colonies of *E. coli* and *S. aureus* on NA plates in the presence of 1.0 G, T and 1.0 GT compared with control also was confirmed by spread plate technique under ambient air temperature is shown in Fig. 7. The antibacterial activity increased with increasing the amount of RGO when the TiO_2 is fixed. The results of antibacterial activities of RGO, TiO_2 and its GT composites, were shown in Fig. 7 and 8. For antibacterial, the dyed silk sample caused significant reductions in the number of growing bacteria after 24 h of incubation of 37 °C. For different concentrations of RGO, the colonies of *E. coli* and *S. aureus* always reduce to a relative low level. The minimum colonies concentrations of RGO against the tested bacteria were similar (up to 90%). The bacterial reduction (%) values of *E. coli* (98%) and *S. aureus* (93%) treated with GT composite (Fig. 8).

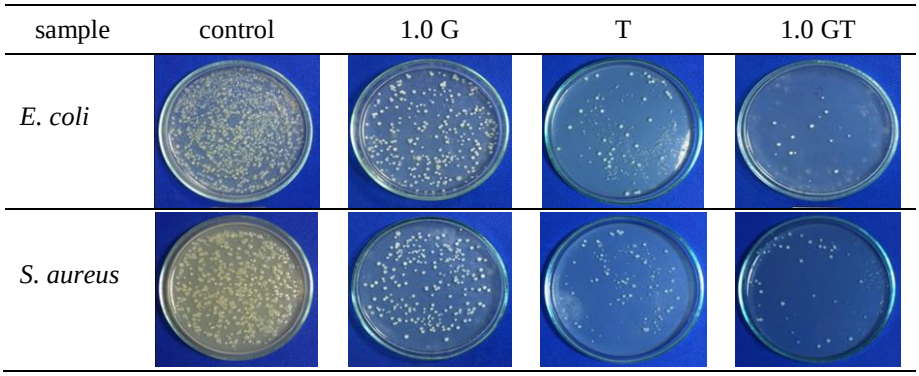

Fig. 7 The results of *E. coli* and *S. aureus* test with composite coated silk fabric.

Fig. 8 shows a higher disinfection of *E.coli* (gram negative bacteria) than that of the *S. aureus* (gram positive bacteria). Mritunjai et al. [37] reported that antibacterial effect was size and dose dependent and more pronounced activity against gram negative bacteria than gram positive bacteria. The bactericidal effect of TiO_2 generally has been attributed to the decomposition of bacterial outer membranes by Reactive Oxygen Species (ROS), primarily hydroxyl radicals (-OH), which leads to phospholipid peroxidation and ultimately cell death [38, 39]. It was proposed that nanomaterials that can physically attach to a cell can be bactericidal if they come into contact with this cell [40]. If the membrane of a bacterium is compromised, the cell may repair itself or, if the scratch is severe, the cell component may release and eventually the cell will die [41]. The impact of nanomaterials on living cells, including bacteria, can also be elucidated by the interactions between the nanomaterial and the individual cell components. The first interaction between a material and a cell is at the membrane interface; some nanoparticles were suggested to embed themselves in the cell membrane [42]. These results confirmed that

the symbiotic effect of RGO and TiO_2 was responsible for the observed strong bactericidal efficiency. Moreover, the absence of oxide functional groups on the edges of the graphene sheets presents a stronger interaction between the more sharpened edges of the reduced nanowalls with the cell membrane of the bacteria and/or a better charge transfer between the bacteria and the edge of the reduced nanowalls, which finally resulted in further damage of the bacterial cell membrane during the contact interaction [43]. Our results are similar to the study on using only GO and RGO papers, which inhibited the growth of *E. coli* where cellular damage of *E. coli* might arise from the effects of either oxidative stress or physical disruption that have been observed in cellular effects of related carbon nanomaterials [43].

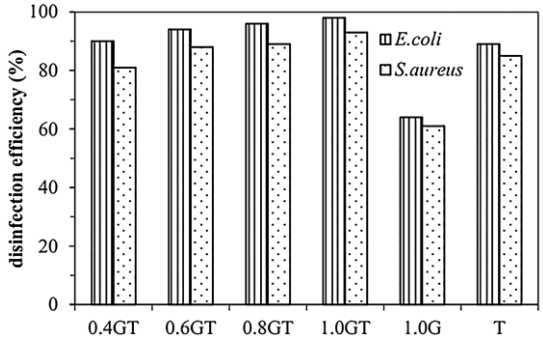

Fig. 8 The disinfection efficiency rate of *E. coli* and *S. aureus* treated with composite materials coated silk fabrics.

Conclusion

RGO and TiO_2 nanocomposites coated on silk fabrics at different RGO ratios were fabricated via a using the modified Hummer's method using TTIP as precursors. RGO having both hydrophilic and hydrophobic functional groups was successfully grafted on fabrics surfaces at loading amounts using 0.4 to 1 mg ml^{-1}. Silk fabrics can be included to have high hydrophobic surface by casing them with the mixture of RGO 1 mg ml^{-1} and TiO_2. Hydrophobicity was achieved due to the lowering of interfacial energy of the fabric surface by the hydrophobic domains present on the RGO as well as offer effective antibacterial activity against on *E.coli* and *S. aureus*. This result indicates that nanocomposite contains high reactive oxygen species and hydroxyl radical contents. We also confirmed that nanocomposites exhibited the enhanced functionality of the self-cleaning and antibacterial activities for coating layers on silk fabrics.

Acknowledgements

This investigation was supported by the Faculty of Engineering, Rajamangala University of Technology Srivijaya, Songkhla, Thailand. We would like also to acknowledge the Materials Engineering Research Center (MERC), Faculty of Engineering, Prince of Songkla University for their facility supports.

References

[1] J. Yang, Z. Zhang, X. Men, X. Xu, X. Zhu, A simple approach to fabricate superoleophobic coatings, New J. Chem. 35 (2011) 576 – 80.

[2] D. Wu, M. Long, J. Zhou, W. Cai, X. Zhu, C. Chen, Y. Wu, Synthesis and characterization of self-cleaning cotton fabrics modified by TiO_2 through a facile approach, Surf. Coat. Technol. 203 (2009) 3728 – 3733.

[3] D. Wu, M. Long, Low-temperature synthesis of N-TiO_2 sol and characterization of N-TiO_2 coating on cotton fabrics, Surf. Coat. Technol. 206 (2012) 3196 – 3200.

[4] B. Tan, B. Gao, J. Guo, X. Guo, M. Long, A comparison of TiO2 coated self-cleaning cotton by the sols from peptizing and hydrothermal routes, Surf. Coat. Technol. 232 (2013) 26 – 32.

[5] K. Qi, J.H. Xin, Room-temperature synthesis of single-phase anatase TiO_2 by aging and its self-cleaning properties, ACS Appl. Mater. Interfaces. 2 (2010) 3479 – 3485.

[6] S. Afzal, W.A. Daoud, S.J. Langford, Photostable Self-Cleaning Cotton by a Copper (II) Porphyrin /TiO_2 Visible-Light Photocatalytic System, ACS Appl. Mater. Interfaces. 5 (2013) 4753 – 4759.

[7] M. Yu, Z. Wang, H. Liu, S. Xie, J. Wu, H. Jiang, J. Zhang, L. Li, J. Li, Laundering Durability of Photocatalyzed Self-Cleaning Cotton Fabric with TiO_2 Nanoparticles Covalently Immobilized, ACS Appl. Mater. Interfaces. 5 (2013) 3697 – 3703.

[8] Q. Xiang, J. Yu, M. Jaroniec, Graphene-based semiconductor photocatalysts, Chem. Soc. Rev. 41 2012 782 – 796.

[9] T. Nakamura, T. Ichitsubo, E. Matsubara, A. Muramatsu, N. Sato, H. Takahashi, On the preferential formation of anatase in amorphous titanium oxide film, Scr. Mater. 53 (2005) 1019 – 1023.

[10] J. Yang, D. Li, X. Wang, X. Yang, L. Lu, Rapid synthesis of nanocrystalline TiO_2/SnO_2 binary oxides and their photoinduced decomposition of methyl orange, J. Solid State Chem. 165 (2002) 193 – 198.

[11] Y.H. Zhang, A. Reller, Phase transformation and grain growth of doped nanosized titania, Mater. Sci. Eng. C. 19 (2002) 323 – 326.

[12] T. Matsunaga, R. Tomada, T. Nakajima, H. Wake, Photoelectrochemical sterilization of microbial cells by semiconductor powders, FEMS Microbiol. Lett. 29 (1985) 211 – 214.

[13] B.S. Necula, L.E. Fratila-Apachitei, S.A.J. Zaat, I. Apachitei, J. Duszczyk, In vitro antibacterial activity of porous TiO_2-Ag composite layers against methicillin-resistant *Staphylococcus aureus*, Acta Biomater. 5 (2009) 3573 – 3580.

[14] S. Sinha, T. Murugesan, K. Maiti, J.R. Gayen, B. Pal and M. Pal, Antibacterial activity of Bergenia ciliata rhizome, Fitoterapia, 72 (2001) 550 – 552.

[15] R. Long, Understanding the electronic structures of graphene quantum dot hysisorption and chemisorption onto the TiO_2 (110) surface: a first-principles calculation, Chem. Phys. Chem, 14 (2013) 579 – 582.

[16] W. Geng, H.X. Liu, X.J. Yao, Enhanced photocatalytic properties of titania-graphene nanocomposites: a density functional theory study. Phys. Chem. Chem. Phys. 15 (2013) 6025 – 6033.

[17] Y. Zhang, Z. Zhou, T. Chen, H. Wang, W. Lu, Graphene TiO_2 nanocomposites with high photocatalytic activity for the degradation of sodium pentachlorophenol. J. Environ. Sci. 26 (2014) 2114 – 2122.

[18] Q. Sun, W. Li, B. Su, Highly hydrophobic solid contact based on graphene-hybrid nanocomposites for all solid state potentiometric sensors with well-formulated phase boundary potentials, J. Electroanal. Chem. 740 (2015) 21 – 27.

[19] B. Xu, J. Ding, L. Feng, Y. Ding, F. Ge, Z. Cai, Self-cleaning cotton fabrics via combination of photocatalytic TiO_2 and superhydrophobic SiO_2, Surf. Coat. Technol. 262 (2015) 70 – 76.

[20] N.D. Tissera, R.N. Wijesena, J.R. Perera, K.N. de Silva, A.J. Gehan, Amaratunge, Hydrophobic cotton textile surfaces using an amphiphilic graphene oxide (GO) coating, Appl. Surf. Sci. 324 (2015) 455 – 463.

[21] D.C. Marcano, D.V. Kosynkin, J.M. Berlin, A. Sinitskii, Z.Z. Sun, A. Slesarev, L.B. Alemany, W. Lu, J. M. Tour, Improved Synthesis of Graphene Oxide, ACS Nano. 4 (2010) 4806 – 4814.

[22] C.K. Chua, M. Pumera, Chemical reduction of graphene oxide: a synthetic chemistry viewpoint, Chem. Soc. Rev. 43 (2014) 291 – 312.

[23] M.J. Ferna´ndez-Merino, L. Guardia, J.I. Paredes, S. Villar-Rodil, P. Solı´s-Ferna´ndez, A. Martı´nez-Alonso, J.M.D. Tasco´n, Vitamin C Is an Ideal Substitute for Hydrazine in the Reduction of Graphene Oxide Suspensions, J. Phys. Chem. C. 114 (2010) 6426 – 6432.

[24] X. Zhu, Q. Liu, X. Zhu, C. Li, M. Xu, Y. Liang, Reduction of Graphene Oxide Via Ascorbic Acid and Its Application for Simultaneous Detection of Dopamine And Ascorbic Acid, Int. J. Electrochem. Sci. 7 (2012) 5172 – 5184.

[25] H.L. Qin, G.B. Gu, S. Liu, Preparation of nitrogen-doped titania with visible-light activity and its application, C. R. Chim. 11 (2008) 95 – 100.

[26] Y. Wang, S. Chou, H.K. Liu, S.X. Dou, Reduced graphene oxide with superior cycling stability and rate capability for sodium storage, Carbon. 57 (2013) 202 – 208.

[27] G. Yang, Z. Jiang, H. Shi, M.O. Jones, T. Xiao, P.P. Edwards, Z. Yan, Study on the photocatalysis of F-S co-doped TiO_2 prepared using solvothermal method, Appl. Catal. B. 96 (2010) 458 – 465.

[28] Z. Ni, Y. Wang, T. Yu, Z. Shen, Raman spectroscopy and imaging of graphene, Nano Res. 1 (2008) 273 – 291.

[29] A.C. Ferrari, Raman spectroscopy of graphene and graphite: Disorder, electron-phonon coupling, doping and nonadiabatic effects, Solid State Commun. 143 (2007) 47 – 57.

[30] J.C. Charlier, P.C. Eklund, J. Zhu, A.C. Ferrari, Electron and phonon properties of graphene: their relationship with carbon nanotubes, In Carbon nanotubes, Springer Berlin Heidelberg. 111 (2007) 673 – 709.

[31] Y. Xu, H. Bai, G. Lu, C. Li, G. Shi, Flexible graphene films via the filtration of water soluble noncovalent functionalized graphene sheets, J. Am. Chem. Soc. 130 (2008) 5856 – 5857.

[32] R. Linker, I. Shmulevich, A. Kenny, A. Shaviv, Soil identification and chemometrics for direct determination of nitrate in soils using FTIR-ATR mid-infrared spectroscopy, Chemosphere. 61 (2005) 652 – 658.

[33] L. Sikong, M. Masae, K. Kooptarnond, W. Taweepreda, F. Saito, Improvement of hydrophilic property of rubber dipping former surface with Ni/B/TiO_2 nano-composite film, Appl. Surf. Sci. 258 (2012) 4436 – 4443.

[34] M. Aleksandrzak, P. Adamski, W. Kukułka, B. Zielinska, E. Mijowska, Effect of graphene thickness on photocatalytic activity of TiO_2-graphene nanocomposites, Appl. Surf. Sci. 331 (2015) 193 – 199.

[35] M. Shahid, A. Ahmad, M. Yusuf, M.I. Khan, S.A. Khan, N. Manzoor, F. Mohammad, Dyeing, fastness and antimicrobial properties of woolen yarns dyed with gallnut (*Quercus infectoria* Oliv.) extract, Dyes Pigm. 95 (2012) 53 – 61.

[36] Z. Bin, W. Lu, L. Liangfei, W.K. Martin, Natural dye extracted from Chinese gall e the application of color and antibacterial activity to wool fabric, J. Cleaner Prod. 80 (2014) 204 – 210.

[37] M. Singh, S. Singh, S. Prasad, I.S. Gambhir, Nanotechnology in medicine and antibacterial effect of silver nanoparticles, Digest Journal of Nanomaterials and Biostructures. 3 (2008) 115 – 122.

[38] M. Cho, H. Chung, W. Choi, J. Yoon, Different inactivation behaviors of MS-2 phage and *Escherichia coli* in TiO_2 photocatalytic disinfection, Appl. Environ. Microbiol. 71 (2007) 270 – 275.

[39] V. Nadtochenko, N. Denisov, O. Sarkisov, D. Gumy, C. Pulgarin, J. Kiwi, Laser kinetic spectroscopy of the interfacial charge transfer between membrane cell walls of *E. coli* and TiO_2, J. Photochem. Photobiol. A. 181 (2006) 401 – 407.

[40] H.A. Jeng, J. Swanson, Toxicity of metal oxide nanoparticles in mammalian cells, J. Environ. Sci. Health, Part A: Toxic/Hazard. Subst. Environ. Eng. 41 (2006) 2699 – 2711.

[41] D.Y. Lyon, A. Thill, J. Rose, P.J.J. Alvarez, Ecotoxicological impacts of nanomaterials. In: M.R. Wiesner, J.Y. Bottero, editors, Environmental Nanotechnology. Applications and Impacts of Nanomaterials, New York, 2007, pp. 445 – 479.

[42] H. Jang, L.E. Pell, B.A. Korgel, D.S. English, Photoluminescence quenching of silicon nanoparticles in phospholipid vesicle bilayers, J. Photochem. Photobiol. A. 158 (2003) 111 – 117.

[43] H.N. Lim, N.M. Huang, C.H. Loo, Facile preparation of graphene-based chitosan films: Enhanced thermal, mechanical and antibacterial properties, J. Non-Cryst. Solids. 358 (2012) 525 – 530.